

The kaobook class

Use this document as a template

Millikelvin Confocal Microscopy of Semiconductor Membranes and Filter Functions for Unital Quantum Operations

Customise this page according to your needs

Tobias Hangleiter*

July 13, 2025

* A \LaTeX lover/hater

The harmony of the world is made manifest in Form and Number, and the heart and soul and all the poetry of Natural Philosophy are embodied in the concept of mathematical beauty.

– D'Arcy Wentworth Thompson

Contents

Contents	iii
I A FLEXIBLE PYTHON TOOL FOR FOURIER-TRANSFORM NOISE SPECTROSCOPY	1
II CHARACTERIZATION AND IMPROVEMENTS OF A MILLIKELVIN CONFOCAL MICROSCOPE	2
III OPTICAL MEASUREMENTS OF ELECTROSTATIC EXCITON TRAPS IN SEMICONDUCTOR MEMBRANES	3
1 Introduction	4
2 The mjolnir measurement framework	5
3 Observations	6
3.1 Transfer-matrix method simulations of the membrane structure	6
4 Conclusion & outlook	12
IV A FILTER-FUNCTION FORMALISM FOR UNITAL QUANTUM OPERATIONS	13
APPENDIX	14
A Additional TMM simulations	15
A.1 Dependence on epoxy thickness	15
A.2 Optimization of the barrier thickness	15
Bibliography	16
List of Terms	17

List of Figures

2.1	Generated by img/tikz/experiment/mjolnir_tree.tex	5
3.1	Generated by img/py/experiment/tmm.py	8
3.2	Generated by img/py/experiment/tmm.py	8
3.3	Generated by img/py/experiment/tmm.py	9
3.4	Generated by img/py/experiment/tmm.py	9
3.5	Sample Honey H13. $\lambda_{\text{exc}} = 795 \text{ nm}$, $P = 1 \mu\text{W}$. Generated by img/py/experiment/pl.py	10
3.6	Sample Doped M1_05_49-2. $V_{\text{CM}} = -1.3 \text{ V}$, $\lambda_{\text{exc}} = 795 \text{ nm}$. Generated by img/py/experiment/pl.py	10
3.7	Sample Fig F10. $\lambda_{\text{exc}} = 795 \text{ nm}$. Generated by img/py/experiment/pl.py	10
3.8	Sample Doped M1_05_49-2. $V_{\text{DM}} = -2.7 \text{ V}$, $V_{\text{CM}} = -1.3 \text{ V}$, $\lambda_{\text{exc}} = 795 \text{ nm}$. Generated by img/py/experiment/pl.py	11
3.9	Sample Doped M1_05_49-2. $V_{\text{B}} = 0 \text{ V}$, Generated by img/py/experiment/pl.py	11
A.1	Generated by img/py/experiment/tmm.py	15
A.2	Generated by img/py/experiment/tmm.py	15

Publications

- [1] Yaiza Aragonés-Soria, René Otten, Tobias Hangleiter, Pascal Cerfontaine, and David Gross. “Minimising Statistical Errors in Calibration of Quantum-Gate Sets.” June 7, 2022. doi: [10.48550/arXiv.2206.03417](https://doi.org/10.48550/arXiv.2206.03417). (Visited on 06/08/2022). Pre-published.
- [2] Pascal Cerfontaine, Tobias Hangleiter, and Hendrik Bluhm. “Filter Functions for Quantum Processes under Correlated Noise.” In: *Physical Review Letters* 127.17 (Oct. 18, 2021), p. 170403. doi: [10.1103/PhysRevLett.127.170403](https://doi.org/10.1103/PhysRevLett.127.170403).
- [3] Thomas Descamps, Feng Liu, Sebastian Kindel, René Otten, Tobias Hangleiter, Chao Zhao, Mihail Ion Lepsa, Julian Ritzmann, Arne Ludwig, Andreas D. Wieck, Beata E. Kardynał, and Hendrik Bluhm. “Semiconductor Membranes for Electrostatic Exciton Trapping in Optically Addressable Quantum Transport Devices.” In: *Physical Review Applied* 19.4 (Apr. 28, 2023), p. 044095. doi: [10.1103/PhysRevApplied.19.044095](https://doi.org/10.1103/PhysRevApplied.19.044095). (Visited on 04/28/2023).
- [4] Thomas Descamps, Feng Liu, Tobias Hangleiter, Sebastian Kindel, Beata E. Kardynał, and Hendrik Bluhm. “Millikelvin Confocal Microscope with Free-Space Access and High-Frequency Electrical Control.” In: *Review of Scientific Instruments* 95.8 (Aug. 9, 2024), p. 083706. doi: [10.1063/5.0200889](https://doi.org/10.1063/5.0200889). (Visited on 08/12/2024).
- [5] Denny Dütz, Sebastian Kock, Tobias Hangleiter, and Hendrik Bluhm. “Distributed Bragg Reflectors for Thermal Isolation of Semiconductor Spin Qubits.” In preparation.
- [6] Sarah Fleitmann, Fabian Hader, Jan Vogelbruch, Simon Humpohl, Tobias Hangleiter, Stefanie Meyer, and Stefan van Waasen. “Noise Reduction Methods for Charge Stability Diagrams of Double Quantum Dots.” In: *IEEE Transactions on Quantum Engineering* 3 (2022), pp. 1–19. doi: [10.1109/TQE.2022.3165968](https://doi.org/10.1109/TQE.2022.3165968).
- [7] Fabian Hader, Jan Vogelbruch, Simon Humpohl, Tobias Hangleiter, Chimezie Eguzo, Stefan Heinen, Stefanie Meyer, and Stefan van Waasen. “On Noise-Sensitive Automatic Tuning of Gate-Defined Sensor Dots.” In: *IEEE Transactions on Quantum Engineering* 4 (2023), pp. 1–18. doi: [10.1109/TQE.2023.3255743](https://doi.org/10.1109/TQE.2023.3255743).
- [8] Tobias Hangleiter, Pascal Cerfontaine, and Hendrik Bluhm. “Filter-Function Formalism and Software Package to Compute Quantum Processes of Gate Sequences for Classical Non-Markovian Noise.” In: *Physical Review Research* 3.4 (Oct. 18, 2021), p. 043047. doi: [10.1103/PhysRevResearch.3.043047](https://doi.org/10.1103/PhysRevResearch.3.043047). (Visited on 01/19/2022).
- [9] Tobias Hangleiter, Pascal Cerfontaine, and Hendrik Bluhm. “Erratum: Filter-function Formalism and Software Package to Compute Quantum Processes of Gate Sequences for Classical Non-Markovian Noise [Phys. Rev. Research 3, 043047 (2021)].” In: *Physical Review Research* 6.4 (Oct. 16, 2024), p. 049001. doi: [10.1103/PhysRevResearch.6.049001](https://doi.org/10.1103/PhysRevResearch.6.049001). (Visited on 10/16/2024).
- [10] Isabel Nha Minh Le, Julian D. Teske, Tobias Hangleiter, Pascal Cerfontaine, and Hendrik Bluhm. “Analytic Filter-Function Derivatives for Quantum Optimal Control.” In: *Physical Review Applied* 17.2 (Feb. 2, 2022), p. 024006. doi: [10.1103/PhysRevApplied.17.024006](https://doi.org/10.1103/PhysRevApplied.17.024006). (Visited on 02/03/2022).
- [11] Paul Surrey, Julian D. Teske, Tobias Hangleiter, Pascal Cerfontaine, and Hendrik Bluhm. “Data-Driven Qubit Characterization and Optimal Control Using Deep Learning.” In preparation.
- [12] Kui Wu, Sebastian Kindel, Thomas Descamps, Tobias Hangleiter, Jan Christoph Müller, Rebecca Rodrigo, Florian Merget, Hendrik Bluhm, and Jeremy Witzens. “An Efficient Singlet-Triplet Spin Qubit to Fiber Interface Assisted by a Photonic Crystal Cavity.” In: *The 25th European Conference on Integrated Optics*. Ed. by Jeremy Witzens, Joyce Poon, Lars Zimmermann, and Wolfgang Freude. Cham: Springer Nature Switzerland, 2024, pp. 365–372. doi: [10.1007/978-3-031-63378-2_60](https://doi.org/10.1007/978-3-031-63378-2_60).

- [13] Kui Wu, Sebastian Kindel, Thomas Descamps, Tobias Hangleiter, Jan Christoph Müller, Rebecca Rodrigo, Florian Merget, Beata E. Kardynal, Hendrik Bluhm, and Jeremy Witzens. “Modeling an Efficient Singlet-Triplet-Spin-Qubit-to-Photon Interface Assisted by a Photonic Crystal Cavity.” In: *Physical Review Applied* 21.5 (May 24, 2024), p. 054052. DOI: [10.1103/PhysRevApplied.21.054052](https://doi.org/10.1103/PhysRevApplied.21.054052). (Visited on 08/21/2024).

Software

The following open-source software packages were developed (at least partially) during the work on this thesis.

- [1] Tobias Hangleiter, Isabel Nha Minh Le, and Julian D. Teske, *Filter_functions* version v1.1.3, May 14, 2024. Zenodo. DOI: [10.5281/ZENODO.4575000](https://doi.org/10.5281/ZENODO.4575000).
- [2] Tobias Hangleiter, *Lindblad_mc_tools*.
- [3] Tobias Hangleiter, *Mjolnir*.
- [4] Tobias Hangleiter, Simon Humpohl, Max Beer, and René Otten, *Python-Spectrometer* version 2024.11.1, Nov. 21, 2024. Zenodo. DOI: [10.5281/ZENODO.13789861](https://doi.org/10.5281/ZENODO.13789861).
- [5] Tobias Hangleiter, Simon Humpohl, Paul Surrey, and Han Na We, *Qutil* version 2024.11.1, Nov. 21, 2024. Zenodo. DOI: [10.5281/ZENODO.14200303](https://doi.org/10.5281/ZENODO.14200303).

Part I

**A FLEXIBLE PYTHON TOOL FOR
FOURIER-TRANSFORM NOISE
SPECTROSCOPY**

Part II

CHARACTERIZATION AND IMPROVEMENTS OF A MILLIKELVIN CONFOCAL MICROSCOPE

Part III

**OPTICAL MEASUREMENTS OF
ELECTROSTATIC EXCITON TRAPS IN
SEMICONDUCTOR MEMBRANES**

Introduction

1



The mjolnir measurement framework

2

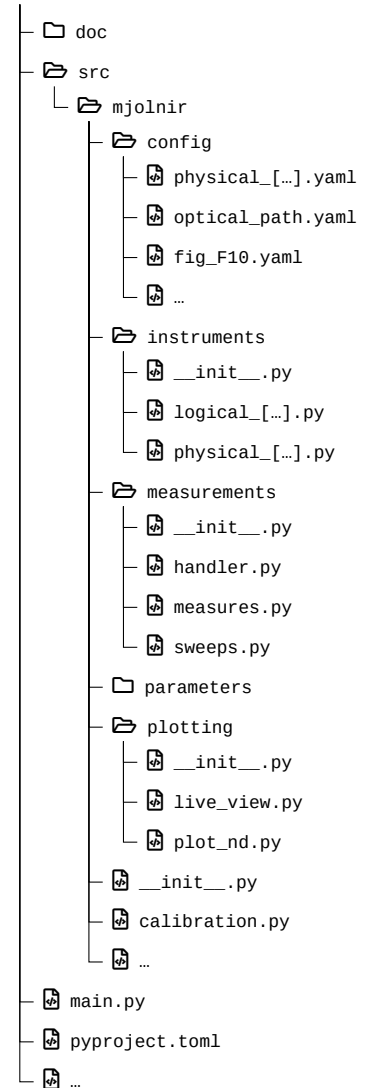


Figure 2.1: Source tree structure of the mjolnir package. Logical QCoDeS instruments and parameters are defined in the instruments and parameters modules, respectively. Instruments are configured using yaml files located in the config directory. The measurements module provides classes for the abstraction of measurements using QCoDeS underneath. Live plots of instrument data as well as a plot function for multidimensional measurement data are defined in the plotting module. calibration.py contains routines for power, CCD, and excitation rejection calibrations. The main.py file is a code cell-based script that serves as the entrypoint for measurements.

3.1 Transfer-matrix method simulations of the membrane structure

The transfer-matrix method (TMM) is a computationally efficient method of obtaining the electric field in layered structures. In this section, I perform simulations of the heterostructure membranes investigated in this part of the present thesis using the PyMoosh package [1] to elucidate the observed quenching of photoluminescence (PL) when illuminating gate electrodes as well as the overall optical efficiency.¹ I will first briefly recap the simulation method following Reference 1. For more details, refer to *ibid.* and references therein.

Consider a layered structure along z with interfaces at $z_i, i \in \{0, 1, \dots, N+1\}$ that is translationally invariant along x and y . Each layer i may consist of a different dielectric material characterized by a (complex) relative permittivity $\epsilon_{r,i}$.² The electric field component along y of a transverse electric (TE) mode originating in some far away point satisfies the Helmholtz equation

$$\frac{\partial^2 E_y}{\partial z^2} + \gamma_i^2 E_y = 0, \quad (3.1)$$

where $\gamma_i = \sqrt{\epsilon_{r,i}k_0^2 - k_x^2}$ with $k_0 = \omega/c$ the wave vector in vacuum and k_x the component along x . In layer i of the structure, the solution to Equation 3.1 may be written as a superposition of plane waves incident and reflected on the lower and upper interfaces [1],

$$\begin{cases} E_{y,i}(z) = A_i^+ \exp\{i\gamma_i[z - z_i]\} + B_i^+ \exp\{-i\gamma_i[z - z_i]\}, \\ E_{y,i}(z) = A_i^- \exp\{i\gamma_i[z - z_{i+1}]\} + B_i^- \exp\{-i\gamma_i[z - z_{i+1}]\}, \end{cases} \quad (3.2)$$

where the coefficients with superscript $+$ ($-$) are referenced to the phase at the upper (lower) interface, respectively. Matching these solutions at $z = z_i$ for all i to satisfy the interface conditions imposed by Maxwell's equations gives rise to a linear system of equations, the solution to which can be obtained through several different methods.

A particularly simple method is the transfer-matrix method (T -matrix formalism), which corresponds to writing the interface conditions at $z = z_i$ as the matrix equation

$$\begin{pmatrix} A_{i+1}^+ \\ B_{i+1}^+ \end{pmatrix} = T_{i,i+1} \begin{pmatrix} A_i^- \\ B_i^- \end{pmatrix} \quad (3.3)$$

with

$$T_{i,i+1} = \frac{1}{2\gamma_{i+1}} \begin{pmatrix} \gamma_i + \gamma_{i+1} & \gamma_i - \gamma_{i+1} \\ \gamma_i - \gamma_{i+1} & \gamma_i + \gamma_{i+1} \end{pmatrix} \quad (3.4)$$

1: Strictly speaking, the term TMM only refers to one of the several formalisms implemented in the PyMoosh package. While fast, it is not the most numerically stable, and other methods may be preferred if wall time is not a limiting issue.

2: We disregard magnetic materials with relative permeability $\mu_r \neq 1$ for simplicity.

the transfer matrix for interface i . Connecting the coefficients for adjacent interfaces within a layer of height $h_i = z_{i+1} - z_i$ requires propagating the phase,

$$\begin{pmatrix} A_i^- \\ B_i^- \end{pmatrix} = C_i \begin{pmatrix} A_i^+ \\ B_i^+ \end{pmatrix}, \quad (3.5)$$

with

$$C_i = \exp \{ \text{diag}(-i\gamma_i h_i, i\gamma_i h_i) \}. \quad (3.6)$$

Iterating Equations 3.4 and 3.6, the total transfer matrix $T = T_{0,N+1}$ then reduces to the matrix product

$$T = T_{N,N+1} \prod_{i=0}^{N-1} T_{i,i+1} C_i. \quad (3.7)$$

From T , the reflection and transmission coefficients can be obtained as $r = A_0^- = -T_{01}/T_{00}$ and $t = B_{N+1}^+ = rT_{10} + T_{11}$. Taking the absolute value square of reflection and transmission coefficients then yields the reflectance \mathcal{R} and the transmittance \mathcal{T} , which correspond to the fraction of total incident power being reflected and transmitted, respectively. To obtain the absorptance \mathcal{A} , the fraction of power being absorbed, in layer i , one can compute the difference of the z -components of the Poynting vectors (*cf.* ??) at the top of layers i and $i+1$. In the TE case considered here, ?? reduces to [1]

$$S_i = \text{Re} \left[\frac{\gamma_i^*}{\gamma_0} (A_i^+ - B_i^+)^* (A_i^+ + B_i^+) \right] \quad (3.8)$$

and is hence straightforward to extract from the calculation of either the S or T matrices.

Equation 3.7 is simple to evaluate on a computer, making this method attractive for numerical applications. However, the opposite signs in the argument of the exponentials in Equation 3.6 can lead to instabilities for evanescent waves ($\gamma_i \in \mathbb{C}$) due to finite-precision floating point arithmetic [2]. Rewriting Equation 3.4 to have incoming and outgoing fields on opposite sides of the equality alleviates this issue while sacrificing the simple matrix-multiplication composition rule in what is known as the scattering matrix (S -matrix) formalism.

Beyond the calculation of the aforementioned coefficients, the TMM formalism also allows to compute the full spatial dependence of the fields. Two cases are implemented in PyMoosh: irradiation of the layered structured with a Gaussian beam rather than plane waves of infinite extent, and a current line source inside the structure. In the first case, the previously assumed translational invariance along x leading to a plane-wave spatial dependence is replaced by a superposition of plane waves weighted with a normally distributed amplitude,³

$$E_{y,i}(x, z) = \exp(ik_x x) \rightarrow \int \frac{dk_x}{2\pi} \mathcal{E}_0(k_x) E_{y,i}(k_x, z) \exp(ik_x x), \quad (3.9)$$

with (*cf.* ??)

$$\mathcal{E}_0(k_x) = \frac{w_0}{2\sqrt{\pi}} \exp \left\{ -ik_x x_0 - \left[\frac{w_0 k_x}{2} \right]^2 \right\} \quad (3.10)$$

3: *I.e.*, the inverse Fourier transform of $\mathcal{E}_0(k_x) E_{y,i}(k_x, z)$.

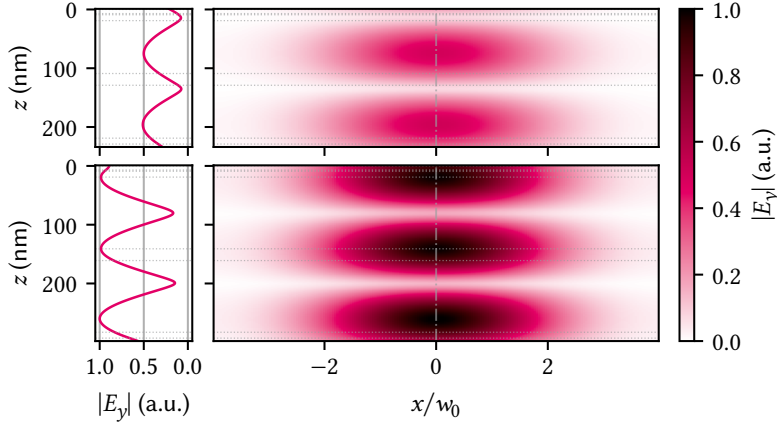


Figure 3.1: Absolute value of the electric field inside the double-gated heterostructure under illumination with a Gaussian beam at $\lambda = 825$ nm from the top. Top (bottom) panels show the structure with the default (optimized) barrier thickness of 90 nm (122 nm), respectively. Dotted horizontal lines indicate interfaces between different materials while the vertical dash-dotted line indicates the position of the line cuts shown in the left column. Increasing the thickness of the barrier has two beneficial effects; first, the overall field intensity inside the structure is higher by a factor of two, and second, there is a peak rather than a knot in the quantum well (QW) at a depth of ~ 120 nm (~ 150 nm), leading to enhanced absorption.

and

$$E_{y,i}(k_x, z) = A_i^- \exp\{i\gamma_i(k_x)[z - z_{i+1}]\} + B_i^+ \exp\{-i\gamma_i(k_x)[z - z_i]\}, \quad (3.11)$$

and where we considered only normal incidence for simplicity.

In the second case, Langevin et al. [1] consider an AC current I flowing through a translationally invariant, one-dimensional wire along y at $x = x_s$. This introduces a source term into the Helmholtz equation Equation 3.1 which, upon Fourier transforming in x direction, leads to

$$\frac{\partial^2 \hat{E}_y}{\partial z^2} + \gamma_i^2 \hat{E}_y = -i\omega\mu_0 I \delta(z) \exp(ik_x x_s). \quad (3.12)$$

The electric field $\hat{E}_{y,i}(k_x, z)$ is thus proportional to the Green's function of Equation 3.12 and can be obtained using a similar procedure as in the case of a distant source incident on the structure by matching the interface conditions. Performing the inverse Fourier transform by means of Equation 3.9 with constant weights, $\mathcal{E}_0(k_x) \equiv 1$, then yields the two-dimensional spatial distribution of the electric field, $E_{y,i}(x, z)$.

Table 3.1

	\mathcal{A} (%)	\mathcal{R} (%)
Bare	2.93	22.43
TG	1.79	41.98
BG	0.50	82.72
TG+BG	0.41	84.78

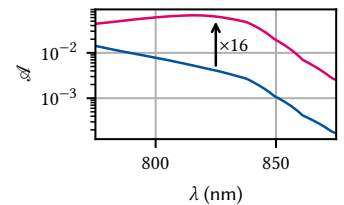


Figure 3.2: QW absorptance \mathcal{A} in a heterostructure with default (blue) and optimized (magenta) barrier thickness and top and bottom gates as function of wavelength. Optimization was performed at 825 nm using the differential evolution algorithm implemented in PyMoosh, resulting in a barrier thickness of 122 nm and an absorptance better by a factor of 16 at 6.3 %.

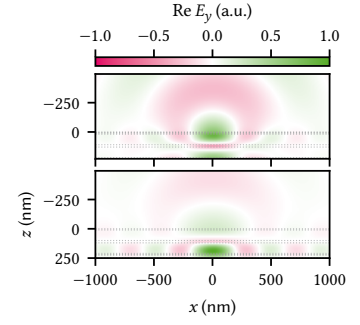


Figure 3.3: Real part of the electric field emitted by a current line located in the QW (black point) for different cases of the unoptimized structure. From top to bottom: bare heterostructure, top gate, bottom gate, top and bottom gate. The half space $z < 0$ is the air above the membrane in the direction of the objective lens and the dotted lines indicate interfaces between materials. Evidently, the bottom gate reduces the amplitude in the upper half of the membrane and thereby the outcoupling efficiency compared to the structures with just a top gate, consistent with what is observed in the experiment.

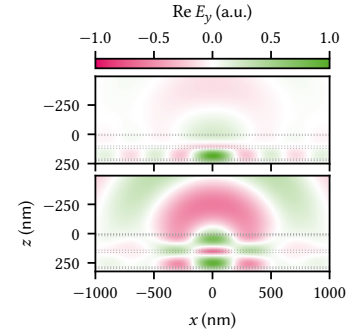


Figure 3.4: Real part of the electric field emitted by a current line located in the QW (black point) for the default (top) and optimized (bottom) structures with top and bottom gates. Optimizing the barrier thickness for absorption in the QW evidently also drastically improves the outcoupling efficiency into the half-space $z < 0$.

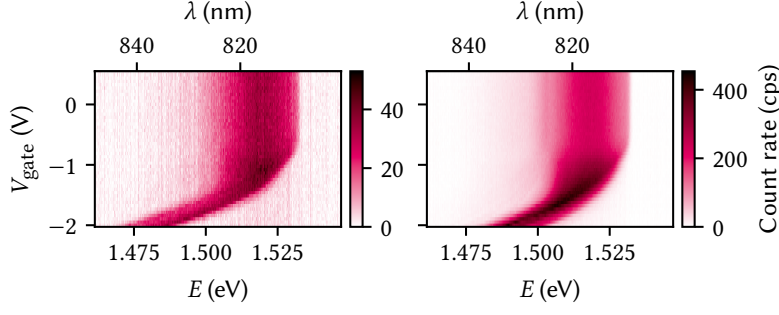


Figure 3.5: PL as function of gate voltage on a single fan-out gate on the bottom (left) and top (right) side of the membrane. The behavior is qualitatively similar but the overall quantum efficiency lower by an order of magnitude for gates on the bottom (as-grown buried) side.

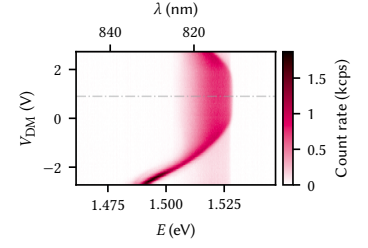


Figure 3.6: PL as function of difference-mode voltage on a large exciton trap. The observed Stark shift follows the expected quadratic dispersion, but is offset by 0.9 V with respect to zero bias (dash-dotted gray line). Remnant PL of the two-dimensional electron gas (2DEG) from outside the trap region is faintly visible below -1 V.

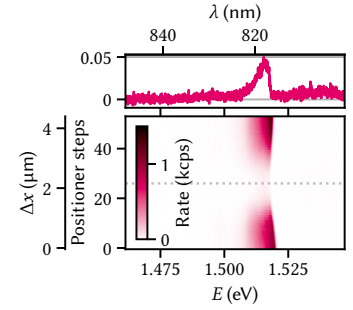


Figure 3.7

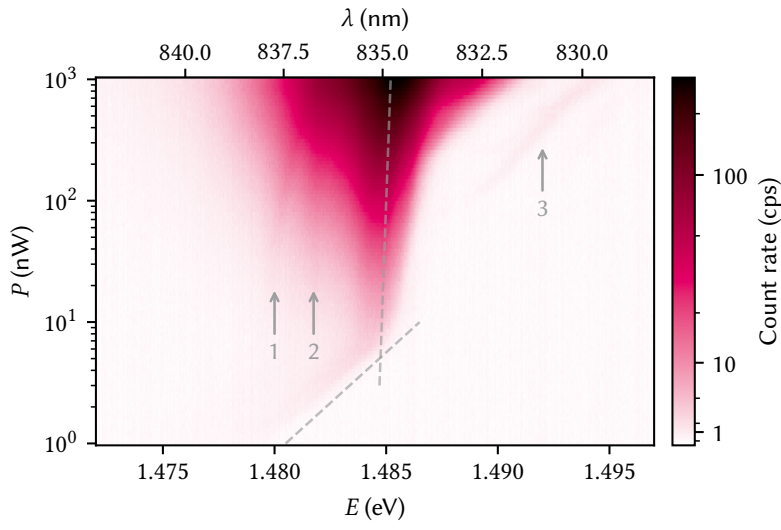


Figure 3.8

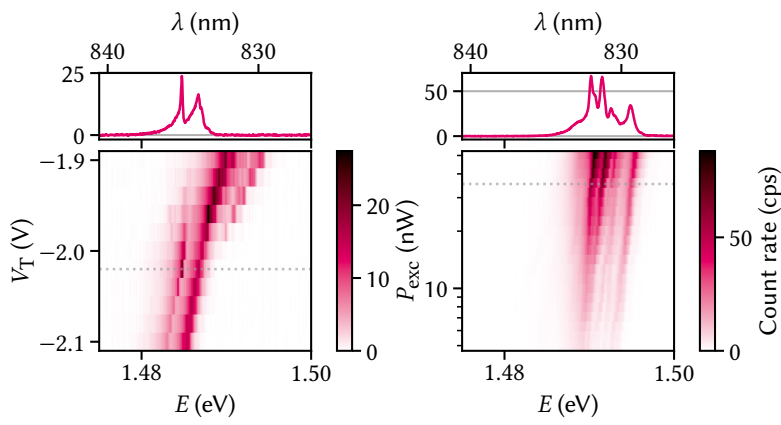


Figure 3.9

Conclusion & outlook

4



Part IV

A FILTER-FUNCTION FORMALISM FOR UNITAL QUANTUM OPERATIONS

APPENDIX

Additional TMM simulations



A.1 Dependence on epoxy thickness

A.2 Optimization of the barrier thickness

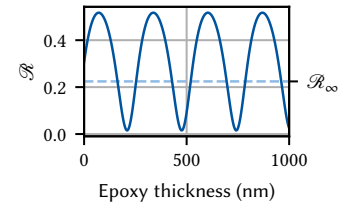


Figure A.1

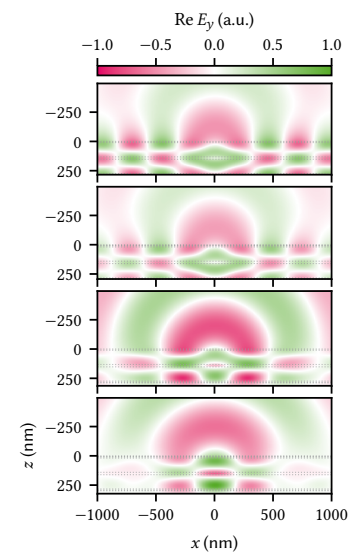


Figure A.2

Bibliography

- [1] Denis Langevin et al. “PyMoosh: A Comprehensive Numerical Toolkit for Computing the Optical Properties of Multilayered Structures.” In: *J. Opt. Soc. Am. B* 41.2 (Feb. 1, 2024), A67. doi: [10.1364/JOSAB.506175](https://doi.org/10.1364/JOSAB.506175). (Visited on 11/11/2024) (cited on pages 6–8).
- [2] Denny Dütz et al. “Distributed Bragg Reflectors for Thermal Isolation of Semiconductor Spin Qubits.” In preparation (cited on page 7).

Special Terms

Symbols

2DEG two-dimensional electron gas. 10

C

CCD charge-coupled device. 5

P

PL photoluminescence. 6, 10

Q

QW quantum well. 8, 9

T

TE transverse electric. 6, 7

TMM transfer-matrix method. 6, 7, 15